Gravity Wave Generation around the Polar Vortex in the Stratosphere Revealed by 3-Hourly Radiosonde Observations at Syowa Station

KAORU SATO

Department of Earth and Planetary Science, The University of Tokyo, Tokyo, Japan

MOTOYOSHI YOSHIKI

The Boston Consulting Group, Tokyo, Japan

(Manuscript received 15 June 2007, in final form 24 December 2007)

ABSTRACT

Intensive radiosonde observations were performed at Syowa Station (69.0°S, 39.6°E) over about 10 days in each of March, June, October, and December 2002 to examine inertia–gravity wave characteristics in the Antarctic lower stratosphere. Based on the 3-hourly observation data, two-dimensional (i.e., vertical wave-number versus frequency) spectra of wind fluctuations were examined, utilizing a double Fourier transform method. Clear signals of gravity waves whose phases propagate upward, suggesting downward energy propagation, are detected in June and October when the polar night jet (PNJ) was present. On the other hand, downward phase propagation (i.e., upward energy propagation) components are dominant in all months. There is a spectral peak around the inertial frequency in a wide range of vertical wavenumbers in December when the background wind was weak, whereas large spectral densities are distributed over lower-frequency regions in June and October. These spectral characteristics are consistent with the results obtained using a gravity wave–resolving global circulation model (GCM) by Sato et al. Dynamical characteristics are examined separately for upward- and downward-propagating gravity waves in June, using a hodograph analysis method. As a result, it is found that upward- and downward-propagating wave packets observed simultaneously in the same height regions have similar horizontal wavelengths and phase velocities. This fact suggests that these gravity waves are generated from the same source with a similar mechanism. When the wave packets were observed, both the local Rossby number and the residual in the nonlinear balance equation estimated using NCEP–NCAR reanalysis data are large around the PNJ situated slightly to the lower latitudes of Syowa Station. Therefore, it is likely that the observed inertia–gravity waves are generated by a spontaneous adjustment around the geostrophically unbalanced PNJ and propagate toward Syowa Station. The possibility of spontaneous gravity wave generation around the PNJ is confirmed by comparison with the GCM simulation by Sato et al.

1. Introduction

Gravity waves are atmospheric waves with a restoring force of buoyancy, which are characterized by their small spatial scales and short periods. Gravity waves have the ability to transport momentum, mostly in the vertical, over a long distance and deposit it in the mean field through dissipation and breaking processes. Since the importance of this ability of gravity waves in the middle atmosphere was recognized in early 1980s, many observational, numerical, and theoretical studies have been performed to elucidate the role of gravity waves in the atmosphere (see Fritts 1984a and Fritts and Alexander 2003 for reviews). Currently gravity waves are recognized as one of primary components of atmospheric dynamics, particularly for the middle atmosphere.

The weak wind layer around the mesopause at middle latitudes is maintained by the mean wind deceleration force associated with the breaking and/or dissipation of gravity waves (Lindzen 1981; Matsuno 1982). Through the downward control principle proposed by Haynes et al. (1991), the gravity wave force drives a global-scale meridional circulation from the summer to winter poles around the mesopause and maintains the

Corresponding author address: Kaoru Sato, Department of Earth and Planetary Science, The University of Tokyo, Tokyo 113-0033, Japan.
E-mail: kaoru@eps.s.u-tokyo.ac.jp

latitudinal gradient of temperature, which is the reverse of what would be expected from the latitudinal distribution of solar radiation. It is also thought that gravity waves may have similar effects on the meridional circulation in the stratosphere (i.e., the Brewer–Dobson circulation), although planetary waves and baroclinic waves are more important in this region (e.g., Plumb 2002). It was shown theoretically (Tanaka and Yamanaka 1985; Palmer et al. 1986; McFarlane 1987) and observationally (Lilly and Kennedy 1973; Sato 1994) that the weak wind layer in the lower stratosphere was partly maintained by topographically forced gravity waves.

In the equatorial middle atmosphere, gravity wave–induced forces do not cause the meridional circulation because the Coriolis force balancing them is negligibly small; rather, they drive characteristic zonal mean zonal wind oscillations such as the quasi-biennial oscillation (QBO) in the lower stratosphere and upper mesosphere and the semiannual oscillation (SAO) in the upper stratosphere and mesosphere (Haynes 1998). Recent studies indicate that the gravity waves, as well as equatorial Kelvin waves and Rossby–gravity waves, are essential for the QBO (Dunkerton 1997; Sato and Dunkerton 1997; Baldwin et al. 2001).

On the other hand, our knowledge of gravity wave sources and properties in the polar region is very much limited because collecting the observations is generally difficult because of harsh natural environments. Gravity wave effects in the polar region are considered a possible key for solving the cold bias in the polar stratosphere, which is one of significant remaining issues of climate models. Moreover, gravity waves in the polar region have an important role in ozone chemistry, which is not observed in the middle- and low-latitude regions. The temperature fluctuations associated with gravity waves can modify the formation and amount of polar stratospheric clouds that control the ozone destruction efficiency (Carslaw et al. 1999; Shibata et al. 2003; Mann et al. 2005; Höpfner et al. 2006; Watanabe et al. 2006).

Sato et al. (1999, hereafter SKT99) simulated gravity waves explicitly using a T106L53 general circulation model (GCM) with an aqua-planet boundary condition. Values of sea surface temperature (SST) climatology in February are given independent of longitude and time (making a perpetual February). Horizontal resolution is about 120 km, and vertical grid spacings are about 600 m in the upper troposphere and lower stratosphere. The reality of the gravity waves was confirmed by comparison with observational winds from the middle and upper (MU) atmosphere radar (Fukao et al. 1985), which is a mesosphere–stratosphere–troposphere (MST)

radar, located at Shigaraki, Japan (34°51′N , 136°06′E). Dominant monochromatic inertia–gravity waves in the lower stratosphere as reported by Sato et al. (1997) using the MU radar observations were well simulated in the model in terms of their amplitudes, vertical wavelengths, and wave periods. It was shown that the frequency spectra of horizontal winds in the lower stratosphere have clear peaks around the inertial frequency at each latitude in the weak wind layer in the lower stratosphere except for the equatorial region, where the inertial frequency approaches zero. Another important finding was the dominance of downward energy flux associated with gravity waves in the polar night jet (PNJ) region, suggesting gravity wave sources in the polar stratosphere.

Yoshiki and Sato (2000) examined seasonal variation of gravity waves in the polar stratosphere using operational radiosonde data from 33 stations over a period of 10 yr. It was shown that both potential and kinetic energies of gravity waves per unit mass are maximized in austral spring at most Antarctic stations, although the maximum is observed in boreal winter in the Arctic, which is similar to the characteristics in middle latitudes. Pfenninger et al. (1999) also reported the spring maximum of gravity wave activity at the South Pole. The spring maximum in the Antarctic seems to be related to the high static stability in association with the polar vortex breaking starting earlier at higher altitudes. Yoshiki et al. (2004) indicate (based on the analysis using original twice-daily operational radiosonde observations at Syowa Station) that the gravity wave energy at Syowa Station becomes large when the PNJ axis approaches the station. Yoshiki and Sato (2000) and Yoshiki et al. (2004) also showed evidence of gravity waves propagating energy downward in winter, which is consistent with the modeling results by SKT99. Possible sources of gravity waves in the polar atmosphere were discussed by Sato (2000).

It is, however, generally difficult to examine upward- and downward-propagating gravity waves separately using operational radiosonde observation data when they are simultaneously present because of too-coarse observational intervals. Thus, in this study, intensive radiosonde observations were performed at 3-h intervals at Syowa Station in the Antarctic in four seasons of 2002 to examine details of gravity wave phase structure both in the vertical and time dimensions. A detailed description of the observations is made in section 2. Seasonal variations of gravity wave activity and the large-scale dynamical structure in the Antarctic stratosphere in 2002 are discussed in section 3. The dominance of downward wave energy propagation is examined in section 4 by using two-dimensional (i.e., vertical

wavenumber versus frequency) spectra. In section 5, dynamical parameters are estimated separately for the downward- and upward-propagating gravity waves in June when the PNJ is stable by analyzing their hodographs. Gravity wave sources are discussed based on the observational evidence, and the results are compared with the GCM results by SKT99 in section 6. Section 7 contains a summary and concluding remarks.

2. Radiosonde observation

Intensive radiosonde (Vaisala RS80–15HG) observations of horizontal winds (by GPS Doppler measurements) and temperature were performed over about 10 days of each season in 2002 at a time interval of 3 h, which is almost the shortest possible when a data receiving system is used. Although the original data sampling time intervals are 2 s, corresponding to about 10-m vertical intervals, we used data with a vertical interval of 50 m made by linear interpolation to make further analysis easier.

There were 80 radiosonde observations for the time period 12–22 March 2002, 84 for 20–30 June, 82 for 16–26 October, and 81 for 5–15 December. October was chosen for the spring period because the gravity wave energy is maximized in this month according to the climatology by Yoshiki and Sato (2000). A few launches failed in June and October because of severe weather conditions.

We also used twice-daily operational radiosonde observation data at Syowa Station (see Yoshiki et al. 2004 for details) and National Centers for Environmental Prediction (NCEP)–National Center for Atmospheric Research (NCAR) reanalysis data covering the time period from February 2002 through January 2003 to examine seasonal variations of gravity wave activity and stratospheric background conditions in 2002.

3. Seasonal variation of the stratosphere in 2002

According to the climatological study for the Antarctic by Yoshiki and Sato (2000), it appears that the seasonal variation of gravity wave activity is related to the polar vortex evolution: the maximum of gravity wave energy is observed in spring when the polar vortex breaking occurs. Thus, we examined the polar vortex evolution based on the latitudinal gradient of potential vorticity (PV) in the time and equivalent latitude section (Fig. 1a) on an isentropic surface of 480 K. The equivalent latitude is defined following Nash et al. (1996). The latitudinal maximum of the PV gradient corresponds roughly to the location of the PNJ. The equivalent latitude of the tangential wind maximum at

each time is denoted by a diamond, and a thick solid curve traces the location of Syowa Station. The intensive observation periods are shown by thick gray bars.

In 2002, an unprecedented major stratospheric warming occurred in the Antarctic (e.g., Hio and Yoden 2005). A sudden poleward shift of the PNJ equivalent latitude is clearly observed in Fig. 1a, corresponding to the sudden warming. Our intensive observation in October was performed after the warming. Thus, the gravity wave characteristics in October 2002 may not be common in the other years. The PNJ was not present in the observation periods in March and December.

On the other hand, the PNJ is dynamically stable in the observation period in June, as seen from Fig. 1a. Syowa Station is located at a slightly higher latitude than the PNJ. Thus, it is expected that typical gravity waves radiated near the PNJ were detected by intensive observations, of which a detailed examination is made in the present study. The data analysis is also performed for the other three time periods, so the unique characteristics of the gravity waves in June can be seen by comparison.

The seasonal variation of gravity wave activity in 2002 is examined by utilizing twice-daily operational radiosonde data at Syowa Station. Figures 1b and 1c show the time series of potential energy per unit mass (PE) and kinetic energy per unit mass (KE) of the fluctuation components, having vertical wavelengths of 2–8 km extracted by a bandpass filter in the height region of 15–25 km in the lower stratosphere, which are considered to be mostly due to gravity waves. It is seen that KE values are generally larger than PE ones throughout the year, suggesting dominance of the inertia–gravity waves (i.e., gravity waves affected by the Coriolis effect). The PE and KE values are mostly large and sporadic in July through November. Gravity wave energy enhancement in association with the major warming, as shown by Venkat Ratnam et al. (2004), is not observed in late September when the PNJ was located far from Syowa Station (Fig. 1a). Instead, large PE and KE values are observed when the PNJ is located near Syowa Station, such as periods in the middle of July, in the middle of September, and in early October. Such a relation between the gravity wave energy and the distance from the PNJ is consistent with the results of Yoshiki et al. (2004). The gravity wave activity in our intensive observation periods is relatively high in March, moderate in June, and weak in October and December.

Figure 2 shows vertical profiles of the time-mean temperature T and the zonal (u) and meridional (v) winds obtained from the intensive radiosonde observations. The tropopause is observed around a height of
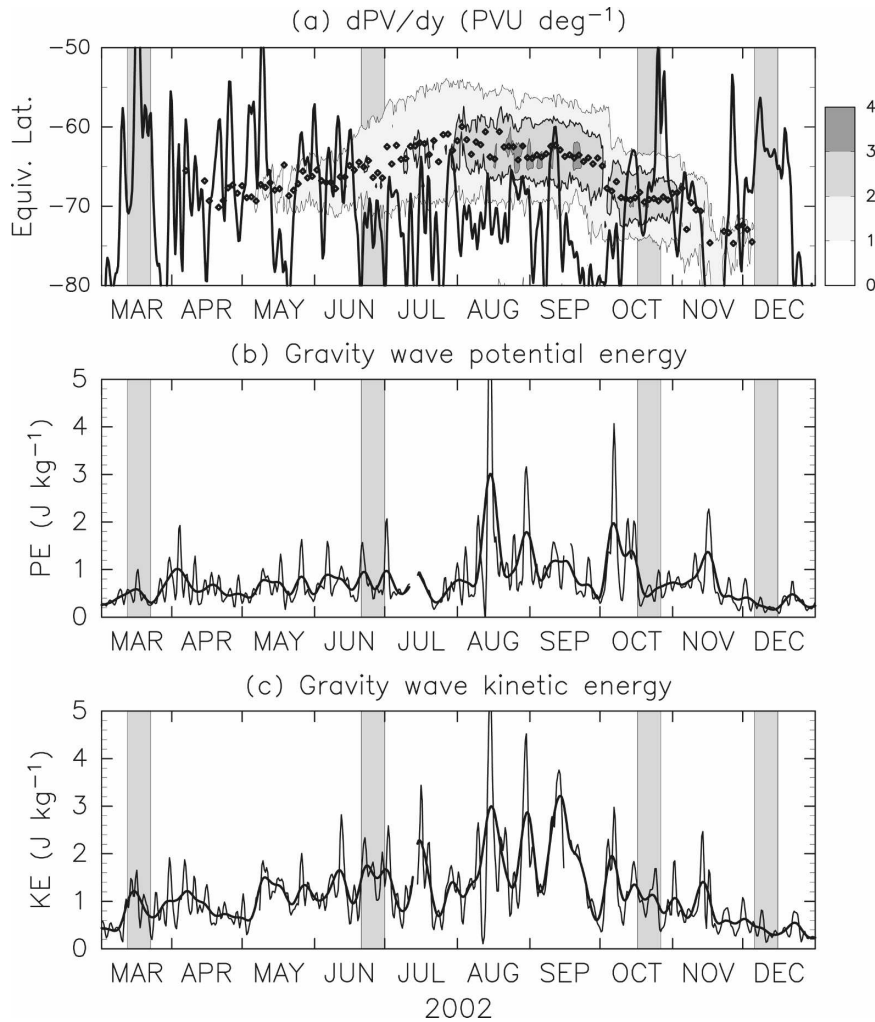
FIG. 1. (a) A time–equivalent latitude section of the latitudinal gradient of potential vorticity on an isentropic surface of 480 K in the Antarctic in 2002 (contours with shading). Contour intervals are 1 PVU ($\equiv 10^{-6}$ K m^2 kg^{-1} s^{-1}) deg^{-1}. Diamonds indicate the equivalent latitude with the maximum PV gradient at each time. A thick solid curve shows the location of Syowa Station. Gray vertical bars indicate intensive radiosonde observation periods. (b), (c) Time series of (b) potential and (c) kinetic energy per unit mass of gravity waves with vertical wavelengths of 2–8 km in the height region of 15–25 km. Thick curves show the time series smoothed with a 5-day running mean.

8–9 km for all profiles. The tropopause structure is clearer in March and December when the polar vortex was not present. The mean temperature in June has its minimum around 20 km; its value is lower than that of the tropopause. The temperature in October is higher than that in March above a height of 18 km. This is because Syowa Station was located outside the polar vortex in the last half observation period in October (Fig. 1a); in other words, middle-latitude warm air intruded into the stratosphere over Syowa Station. Although the intensive observation periods are limited, the vertical profiles of the mean zonal wind show clear seasonal change in the Antarctic stratosphere: the

mean zonal wind is weak but already westerly in March, strongly westerly in June because of the existence of the PNJ, weakened above 20 km in October (corresponding to the polar vortex breaking that starts earlier at higher altitudes), and weakly easterly above 22 km in December (associated with an anticyclone in the polar summer stratosphere). The mean meridional wind is generally weak except above 25 km in June.

4. Frequency–vertical wavenumber spectra in each season

Figure 3 shows time–height sections of zonal and meridional wind anomalies from the time mean in Fig. 2
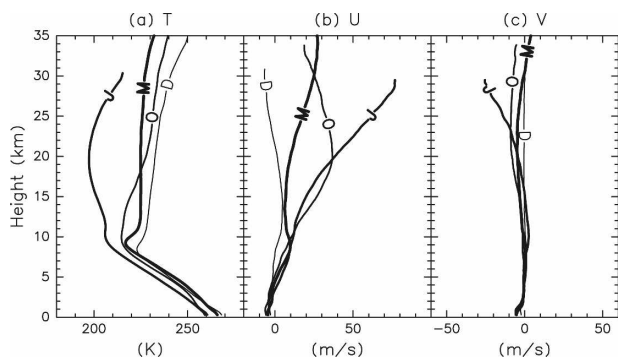
FIG. 2. Temperature and zonal and meridional winds as a function of the geopotential height, averaged for each observation period of March (M), June (J), October (O), and December (D) 2002.

for respective observation periods. In March when the polar vortex is absent, downward phase propagation is dominant for both wind fluctuation components in the whole stratosphere. This is also the case for December. On the other hand, the time–height sections for June when the polar vortex is stable show that both upward and downward phase propagation components are present. Such a mixture of upward- and downward-propagating phases is also observed in October.

To examine statistical characteristics of the phase propagation, we calculated two-dimensional (vertical wavenumber versus frequency) power spectra. First, we removed low-frequency components with a high-pass filter with a cutoff wave period of 42 h. Second, a two-dimensional autocorrelation function was calculated for the height region of 15–30 km and for the whole observation period of each month. Then, the power spectra were obtained by applying a double Fourier transform to the autocorrelation function. The results are shown in Fig. 4 for v components. Thick vertical lines indicate a 1-day period (left) and the inertial period (~13 h at Syowa Station) (right). Because the observed frequency ω is taken to be positive, positive (negative) vertical wavenumbers m indicate upward (downward) phase propagation. According to the gravity wave theory, the downward phase propagation (negative m) means upward energy propagation, when the Doppler effect by the background wind is not significant.

It is clear that negative m components are dominant for all months, particularly for March and December. In December, an isolated peak is observed near the inertial period at almost all vertical wavenumbers. This feature is consistent with the gravity wave spectra shown by SKT99 using a gravity wave–resolving GCM, in which isolated spectral peaks are observed around the inertial periods at most latitudes in a weak wind layer in the lower stratosphere. Such an isolated peak

near the inertial period is also reported by using wind observation data from MST and stratosphere–troposphere (ST) radars (e.g., Sato et al. 1997; Nastrom and Eaton 2006). Another interesting and important feature observed in Fig. 4 is that spectral amplitudes are also large in the positive m region for June and October. Similar features are also observed in u and T spectra (not shown).

It is worth noting here that there are a few points to be considered for the interpretation of the two-dimensional spectra. One is the ambiguity of the sign of "estimated" m originating from the Doppler effect of the mean wind. The ground-based (observed) frequency ω is related to the intrinsic frequency $\hat{\omega}$ by the Doppler relation

$$\omega = \hat{\omega} + k\overline{U}, \quad (1)$$

where $\overline{U}$ is the mean wind in the direction of horizontal wavenumber vector k. The intrinsic frequency $\hat{\omega}$ is taken to be positive without losing generality, which makes theoretical interpretation easier: positive (negative) m means downward (upward) energy propagation (e.g., Sato et al. 1997). The ground-based frequency ω can be negative, however, if the Doppler effect of the mean wind $k\overline{U}$ is largely negative (e.g., Sato 1989; Lintelman and Gardner 1994), following (1). Thus, the Doppler effect may cause the wrong interpretation of vertical energy propagation of gravity waves for the two-dimensional spectra: when the ground-based frequency ω is taken to be positive as in Fig. 4, the sign of the estimated m may become opposite to the real m. However, the Doppler effect is not sufficiently severe to fail the estimation of the sign of m in the present study, as shown by the hodograph analysis made in section 5, even for the most severe case in June.

Another point is a drifting effect. The balloon measurements are not made instantaneously over the whole height region. In the present study, the buoyancy of the balloons was adjusted so they could ascend at a speed of about 5 m s^{-1}, similar to operational observations; hence, the balloons drifted horizontally by the mean wind during the observation. This drifting effect may make observed vertical wavenumbers and wave periods different from the real ones (e.g., Gardner and Gardner 1993; Lane et al. 2000). However, it seems that this effect is not significant in the present study. In June, when the mean wind is most strong, a typical observed vertical wavelength is about 3 km (Fig. 4b). The time period during which a radiosonde observes one cycle of this vertical wavelength is about 10 min. This time period is much shorter than the typical wave period of 14 h (Fig. 4b), so the temporal change of gravity wave
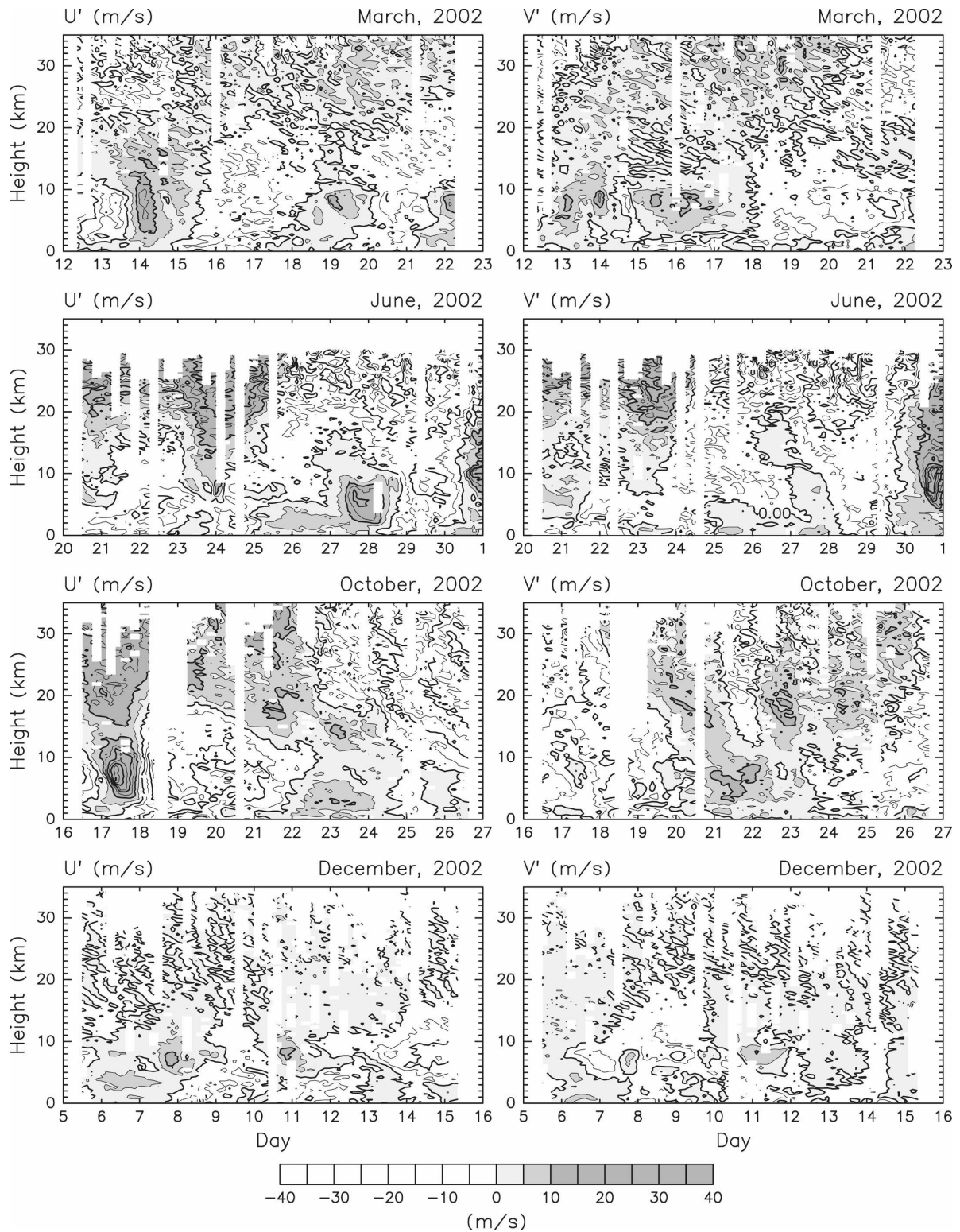
FIG. 3. Time–height sections of wind anomaly from the time mean for each observation period, with (left) zonal and (right) meridional wind fluctuation components. Contour intervals are 5 m s^{-1}.
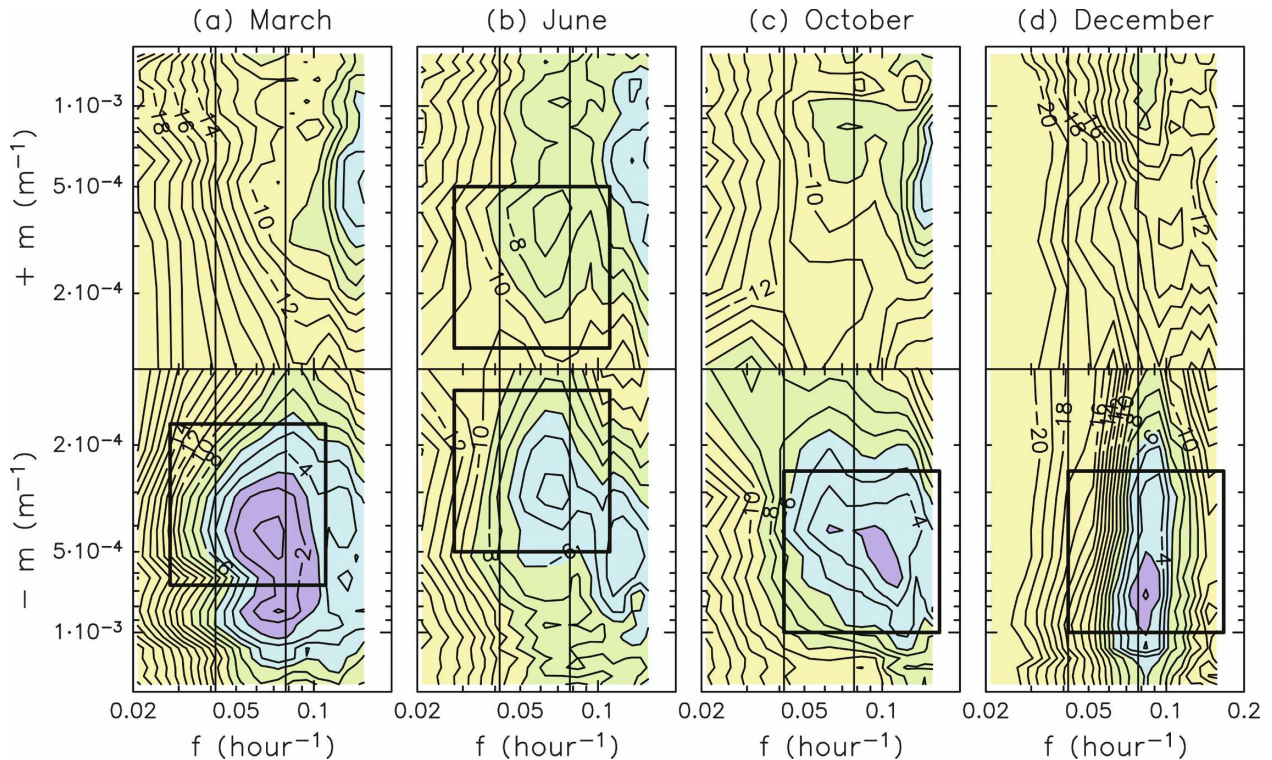
FIG. 4. Frequency vs vertical wavenumber spectra of meridional wind fluctuations for each observation period in the energy content form (i.e., spectral density multiplied by frequency and vertical wavenumber). The units are dB. The contour intervals are 1 dB. Rectangles indicate the domains for which a detailed hodograph analysis was made to estimate gravity wave parameters. The vertical lines indicate (left) the diurnal frequency and (right) the inertial frequency at Syowa Station.

phases during the observation can be ignored. Taking the largest mean wind of about 80 m s^{-1} (Fig. 2) as a worst case, the drifted horizontal distance in 10 min is estimated at about 48 km. This distance is about 15% of a typical horizontal wavelength of about 300 km in June as estimated in section 6a. The errors in the estimates of the vertical wavelength are considered to be a similar percentage. The estimates of the wave period, however, do not suffer from the drifting effect as long as the background winds can be assumed to be steady because the time difference of adjacent observations is almost constant (3 h) at each height level. It is considered that the drifting effect is less significant in the other months when the mean wind is weaker. Therefore, the two-dimensional spectra in Fig. 4 are simply interpreted as follows: Large spectral amplitudes in the negative *m* region in all months in Fig. 4 mean that dominant gravity waves propagate energy upward; and significant peaks observed in the positive *m* region for June and October indicate that there are gravity waves propagating energy downward and suggest that there are gravity wave sources in or above the stratosphere.

5. Wave parameter estimation by 2D hodograph analysis

To examine detailed gravity wave characteristics, we made a hodograph analysis for observed wind fluctuations. Although the hodograph analysis is usually applied to one-dimensional data (e.g., vertical profiles), we made the analysis for two-dimensional hodographs (i.e., time and height variation of horizontal fluctuation vectors), following Sato et al. (1997), because the data obtained in the present study have sufficient resolution to detect both the vertical wavelength and the ground-based wave period directly, as seen in the two-dimensional spectra.

First, we extracted dominant fluctuation components in the frequency and vertical wavenumber domains where spectral peaks were observed (as shown by rectangles in the power spectra in Fig. 4) by bandpass filters. The cutoff frequencies and vertical wavenumbers for each month are listed in Table 1. Second, two-dimensional hodographs were analyzed for the time and height regions with the same lengths of the mean wave period and vertical wavelength of extracted com-

TABLE 1. Ranges of wave period and vertical wavelength for each observation period for the gravity wave analysis.

Month	Wave periods	Vertical wavelengths
March	9–36 h	1.5–6 km
June	9–36 h	2–8 km
October	6–24 h	1–4 km
December	6–24 h	1–4 km

ponents. Analyzed regions were shifted by 3 h in time and 0.5 km in the vertical for the entire observation time period and the height region of 15–30 km; then gravity wave characteristics were estimated in terms of horizontal wavenumbers, horizontal phase velocities, and vertical momentum fluxes, assuming a monochromatic wave. Details are described below.

According to the hydrostatic inertia–gravity wave theory, horizontal wind fluctuations that are parallel to (U') and perpendicular to (V') the horizontal wavenumber vector and the buoyancy fluctuations $\theta'g/\overline{\theta}$, where θ is the potential temperature and g is the gravitational acceleration, are described with the same amplitude scale factor of A:

$$U' = \mathrm{Re}\left[\frac{\hat{\omega}m^2}{kN^2} A \exp i(mz - \omega t + \phi_0)\right], \quad (2)$$

$$V' = \mathrm{Re}\left[\frac{-ifm^2}{kN^2} A \exp i(mz - \omega t + \phi_0)\right], \quad \text{and} \quad (3)$$

$$\frac{\theta'}{\overline{\theta}} g = \mathrm{Re}[imA \exp i(mz - \omega t + \phi_0)], \quad (4)$$

where k is the horizontal wavenumber, f and N are the inertial and buoyancy frequencies, respectively, z is the altitude, t is time, and ϕ_0 is a constant phase at the ground ($z = 0$).

A least-squares fit to a two-dimensional monochromatic sinusoidal wave is applied to wind and temperature fluctuations, and then m, ω, and the horizontal wavenumber direction Θ_0 (the anticlockwise-defined angle from the east) are directly estimated. The intrinsic frequency $\hat{\omega}$ is obtained from the ratio R of short to long axes of the hodograph ellipse, which equals $f/\hat{\omega}$. The horizontal wavenumber k is estimated using the dispersion relation of hydrostatic inertia–gravity waves,

$$\hat{\omega}^2 = f^2 + \frac{k^2}{m^2} N^2. \quad (5)$$

The statistics for the estimated wave parameters are made for trustworthy cases because observational noise and other kinds of disturbances sometimes largely contaminate the hodographs. We used the following criteria: $0.2 < R < 0.9$, the kinetic energy per unit mass is larger than 1 J kg^{-1}, the ground-based wave period $2\pi/\omega$ is longer than 6 h (the Nyquist period for 3-hourly time series), and the residual of the least squares fit is smaller than one half of the estimated kinetic energy per unit mass. The phase at the ground ϕ_0 is estimated independently for wind and temperature fluctuations. Thus, we added another criterion for selection: the difference between the two phases is smaller than 0.5 rad. Finally, because the ω value can be also estimated from the Doppler relation (1) and should accord with directly estimated ω by the least squares fit, we added yet one more criterion for selection: the difference between the two ω estimates is smaller than a third of $k\overline{U}$. Note that the error in ω estimated from (1) is affected by the mean wind $\overline{U}$, which is large in winter.

It is also worth noting that we ignored the effect of vertical shear of the mean wind perpendicular to the horizontal wavenumber vector proposed by Hines (1989) in the present hodograph analysis. For example, the ratio R of short to long axes of the hodograph ellipse is modified in the presence of the vertical shear (e.g., Sato 1994) as in the following:

$$R = \frac{f}{\hat{\omega}} - \frac{V_z k}{m\hat{\omega}}. \quad (6)$$

This effect is significant for gravity waves with higher intrinsic frequencies like topographically forced gravity waves (Hines 1989) because the first term on the right-hand side of (6) is quite small (i.e., almost linear polarization). In the Antarctic, topographically forced gravity waves are hardly able to propagate into the stratosphere in winter because the mean wind near the surface is easterly (see Fig. 2b) and then a critical level exists in the troposphere (Yoshiki and Sato 2000). The most severe case may be the analysis for dominant inertia–gravity waves in June (examined in the next section) because the background wind shear perpendicular to the wave vector is large. In this case, the modification for R by the second term of the right-hand side of (6) was about 20% (not shown in detail). We double-checked the accuracy of estimated wave parameters by comparing the two estimates of ω directly from the time variation of phases and theoretically from the hodograph ellipse as documented above. Thus, it is considered that the statistics shown in this section are not affected largely by the vertical shear effect.

Figure 5 shows the scatter diagram of $\hat{\omega}$ versus the direction of horizontal wavenumber vector relative to the background wind Θ. Crosses and circles show the results of waves with negative m (i.e., upward energy propagation) and positive m (i.e., downward energy propagation), respectively. It is seen that Θ values are
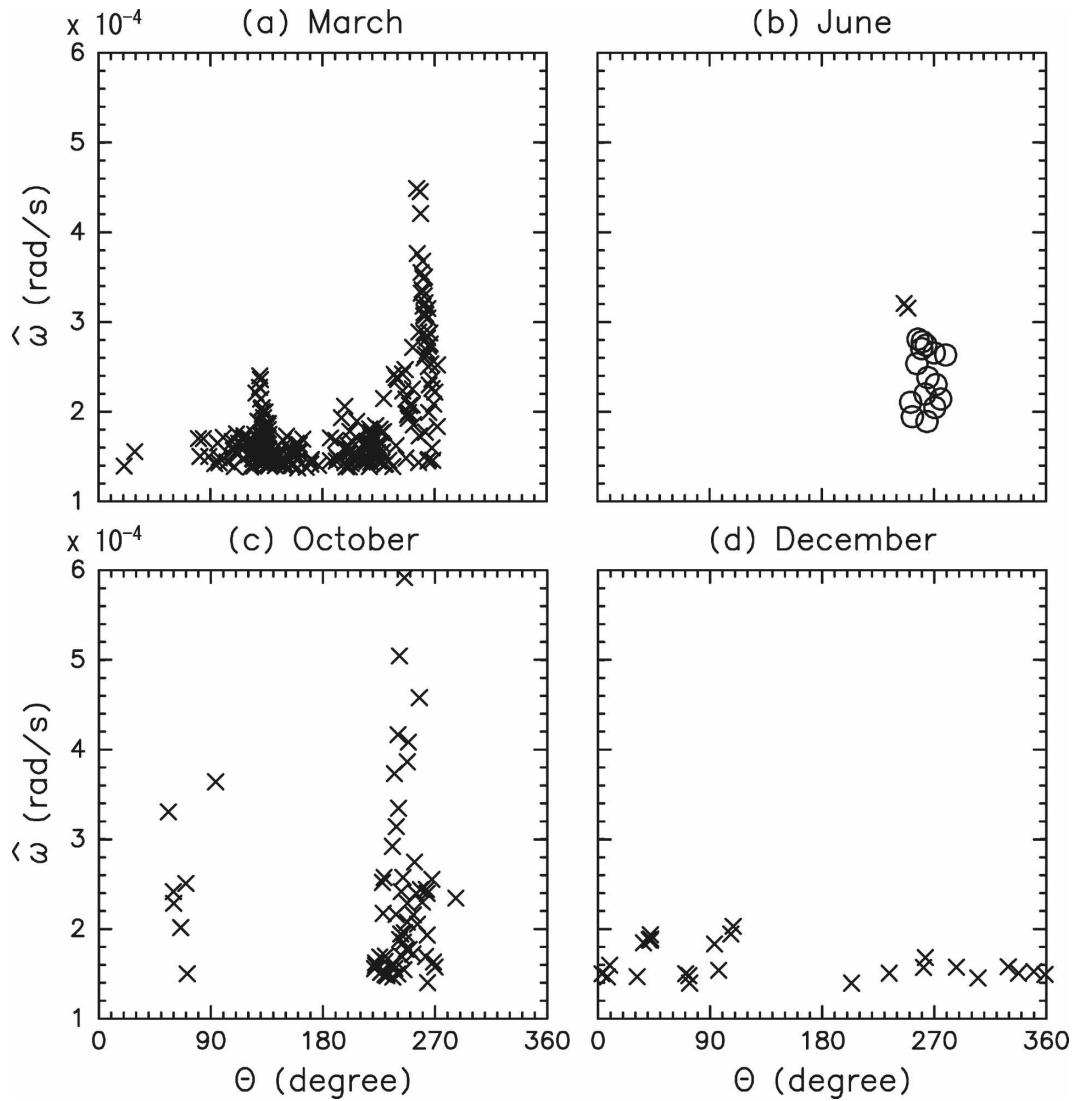
FIG. 5. A scatter diagram of $\hat{\omega}$ vs the direction of horizontal wavenumber vector relative to the background wind Θ for each month. Crosses and circles show results of the waves propagating energy upward and downward, respectively.

distributed around ~270° for waves with relatively large $\hat{\omega}$ in March, June, and October. Because the background winds in these months are almost westerly (Fig. 2), the direction of Θ (~270°) implies poleward propagation. In March, a number of waves are distributed in a region around $\Theta \sim 180°$ and have relatively small $\hat{\omega}$, suggesting that these waves tend to propagate westward relative to the background wind. In December, $\hat{\omega}$ values are small (close to f) and no preferable propagation direction is observed.

The scatter diagram of the ground-based horizontal phase speed versus horizontal wavelength is shown in Fig. 6. Solid lines show the gradient corresponding to the inertial frequency f (~1.4×10^{-4} s^{-1}) at Syowa

Station for reference. An important feature is that there are no negative ground-based phase speeds, which confirms that the Doppler effect is not so significant; that is, all ω values are positive [see (1)]. This fact assures the validity of the interpretation of the two-dimensional spectra regarding the vertical energy propagation in section 4. The dominant horizontal wavelengths are 300–500 km in June and October when the polar vortex is present, whereas waves in March and December are distributed widely in the range of 300–1000 km. Most phase speeds are slower than 15 m s^{-1} in June and October, whereas those in March and December are again distributed widely in the range of 3–30 m s^{-1}.
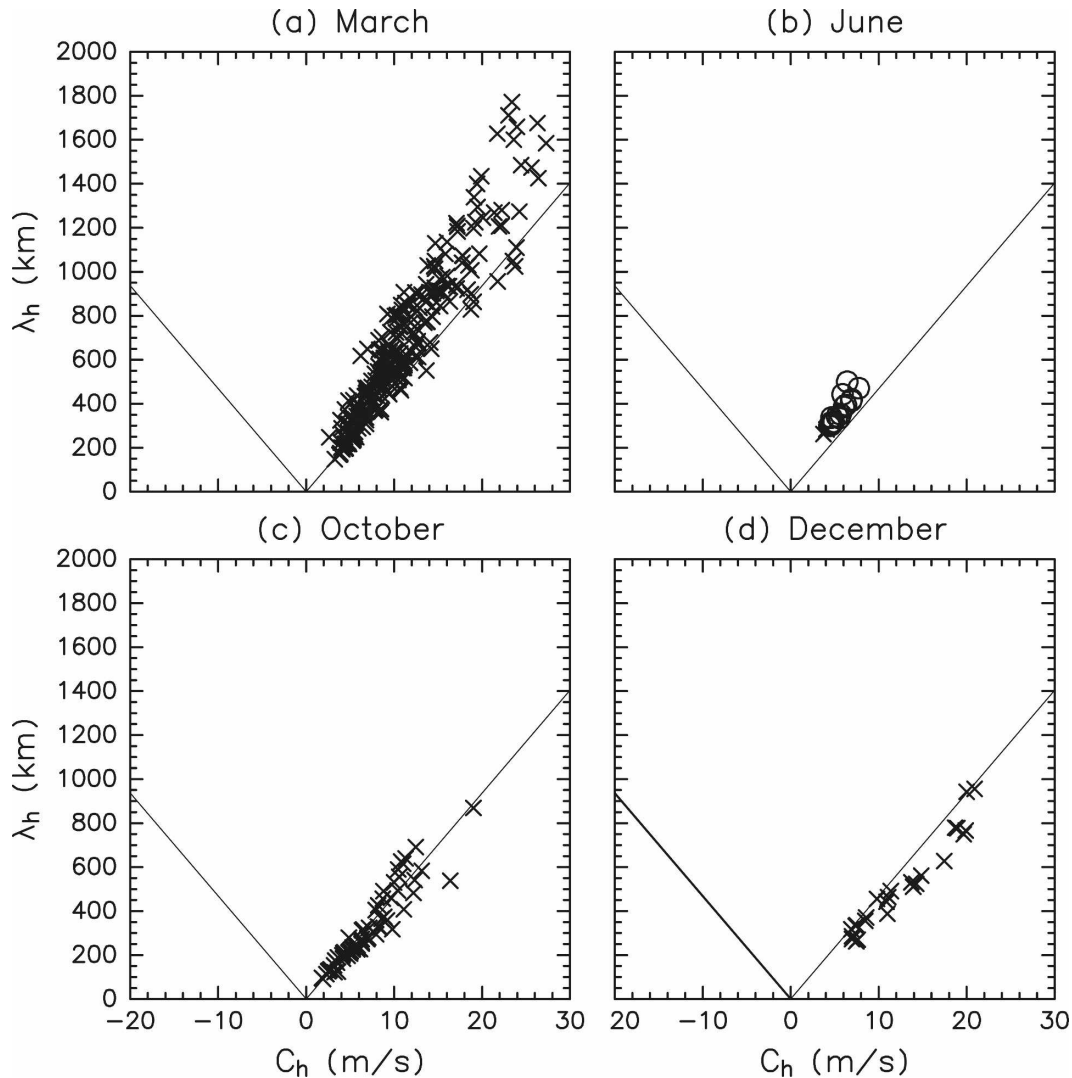
FIG. 6. As in Fig. 5, but for the scatter diagram of the ground-based horizontal phase speed vs horizontal wavelength. Solid lines correspond to the inertial frequency, for reference.

Using parameters obtained by the hodograph analysis, vertical fluxes of zonal and meridional momentum per unit mass can be estimated respectively by assuming uniform background fields

$$\overline{u'w'} = -\text{sgn}(m)\frac{\hat{\omega}}{2N^2}|U'|\left|\frac{\theta'}{\overline{\theta}}g\right|\cos\theta_0 \quad \text{and} \quad (7)$$

$$\overline{v'w'} = -\text{sgn}(m)\frac{\hat{\omega}}{2N^2}|U'|\left|\frac{\theta'}{\overline{\theta}}g\right|\sin\theta_0. \quad (8)$$

Figure 7 shows the distribution of estimated momentum flux vectors. In March, June, and October, most $\overline{u'w'}$ values are negative for waves propagating energy upward (denoted by crosses), which means that these waves propagate westward relative to the background

westerly wind (Fig. 2). Positive $\overline{u'w'}$ values for waves propagating energy downward (denoted by circles) observed in June are also consistent with westward propagation relative to the westerly wind. It is interesting that in December when the background wind is weakly easterly above the height of ~20 km, some waves have positive $\overline{u'w'}$, although the values are small. This feature suggests that the waves propagate eastward relative to the background easterly wind. Thus, we can generalize that observed waves commonly propagate opposite to the background wind in all seasons, independent of the vertical propagation.

Vertical fluxes of meridional momentum $\overline{v'w'}$ tend to be negative (positive) for waves propagating energy upward (downward) in June and October, indicating that
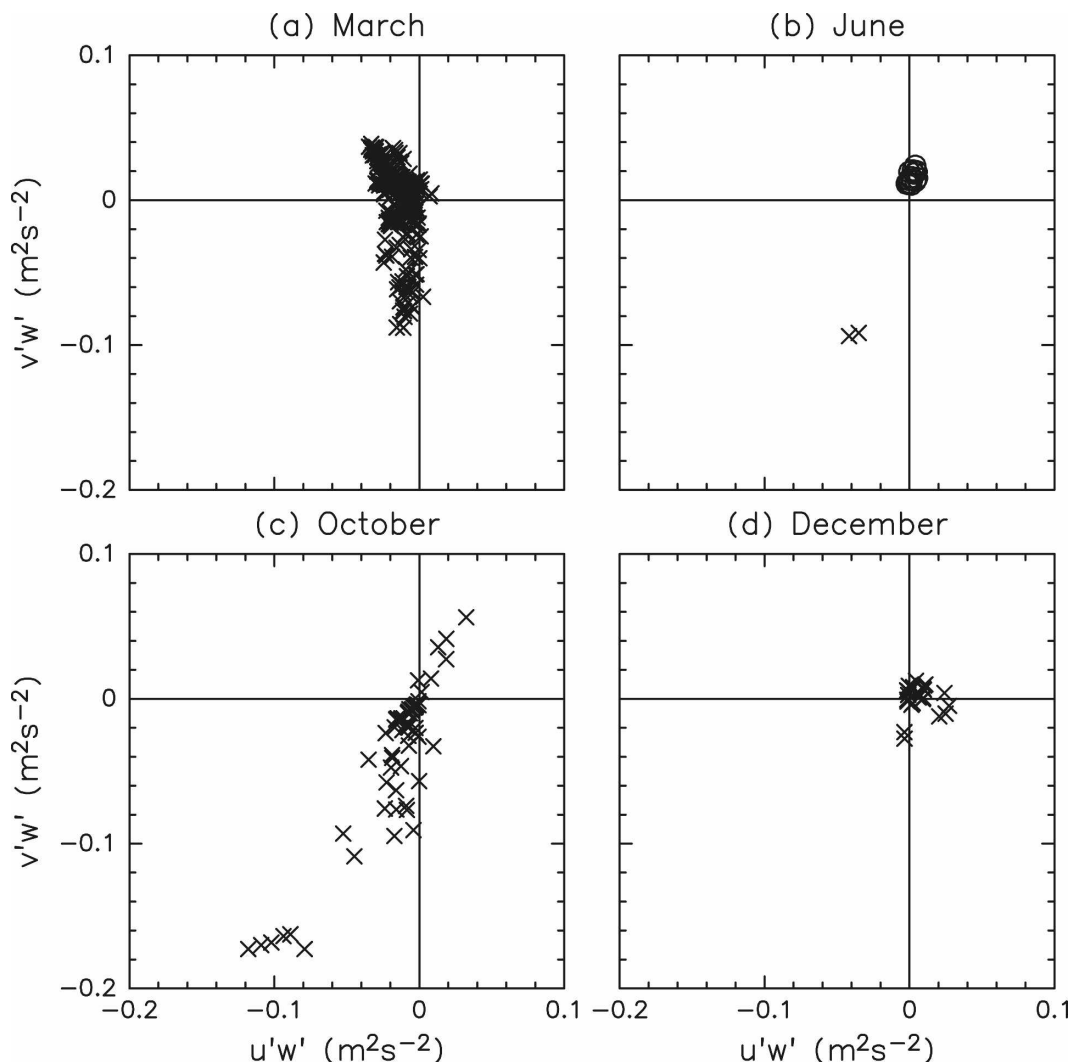
FIG. 7. Vertical fluxes of horizontal momentum estimated by the hodograph analysis for each month. Crosses and circles denote the results for waves propagating energy upward and downward, respectively.

most gravity waves propagate poleward. In March, $\overline{v'w'}$ values have both positive and negative signs, suggesting that there are both kinds of waves propagating equatorward and poleward. The values of $\overline{v'w'}$ are small in December.

6. Gravity wave sources observed in the polar vortex

a. Wave characteristics

The existence of gravity waves propagating energy downward in the stratosphere is a unique feature observed in the polar region (SKT99; Yoshiki and Sato 2000; Yoshiki et al. 2004). Thus, a detailed analysis is made in the present section for gravity waves observed

in June when the PNJ is stable, in terms of the wave structure, the timing of appearance, and the background field characteristics.

The time and height sections of filtered meridional wind fluctuations are separately shown for upward and downward phase propagation components in Fig. 8. An interesting feature is that the regions where wave packets appear accord for both components. Two examples are shown by rectangles placed at the same regions in Figs. 8a and 8b. It is also important that the origins of the wave packets appear to be at almost the same altitudes, as shown by arrows depicting packet propagation.

Figure 9 shows the phase velocities estimated by the hodograph analysis for the region of the rectangle on
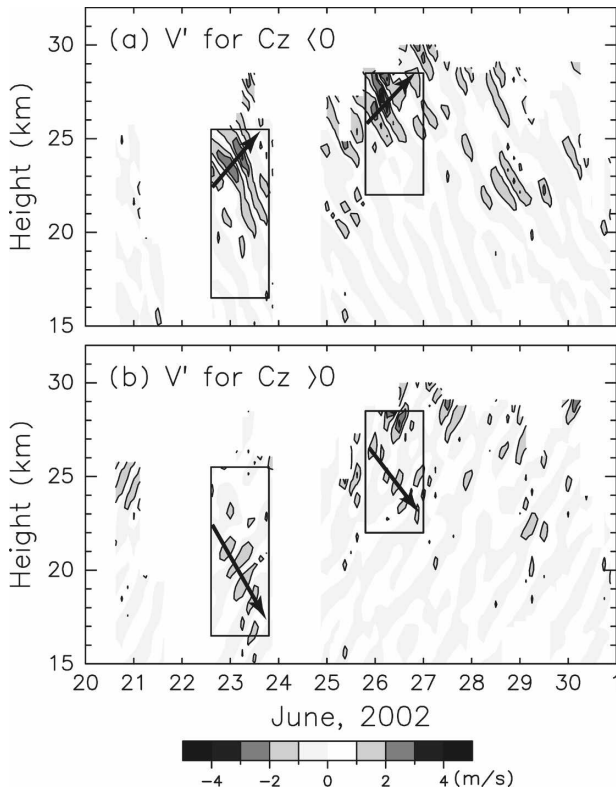
FIG. 8. Time–height sections of (a) upward and (b) downward phase propagation components of meridional wind fluctuations in June. The rectangles denote the regions when and where strong wave packets are observed. Arrows depict the packet propagations.
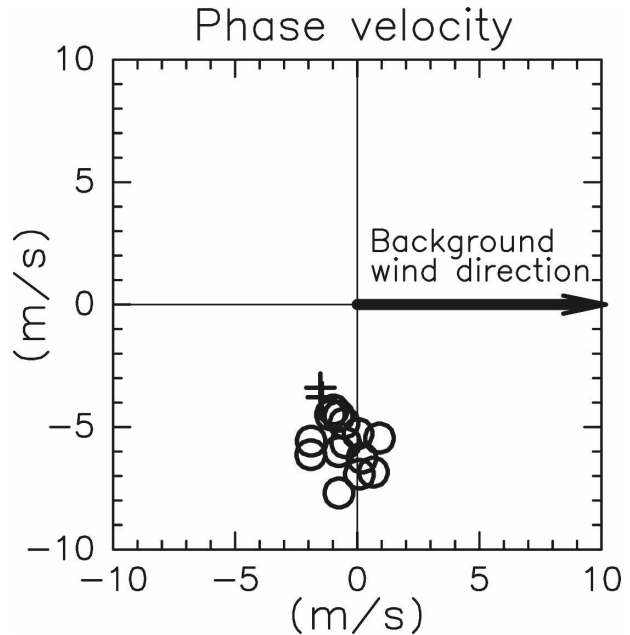

FIG. 9. Ground-based horizontal phase velocities obtained by a hodograph analysis for June. The background wind direction is taken to be rightward. Circles and crosses are the results for upward and downward phase propagation components, respectively.

22–23 June 2002. Phase speeds are about 5 m s^{-1}, independent of the vertical phase propagation direction. The averaged horizontal wavelengths are about 270 and 380 km for upward and downward phase propagation, respectively. Judging from these similar wave characteristics and origins, we can infer that both upward- and downward-propagating waves were generated from the same source with a similar mechanism.

b. Generation mechanisms

A possible source of the gravity waves observed in the Antarctic stratosphere is the spontaneous adjustment around the large-scale polar night jet. O'Sullivan and Dunkerton (1995) produced a pioneering work on the spontaneous generation of gravity waves in the life cycle of baroclinic waves in the troposphere, using a three-dimensional dry hydrostatic model. Zhang (2004), Plougonven and Snyder (2007), and Wang and Zhang (2007) used a nonhydrostatic regional model to examine mesoscale gravity wave generation in upper-tropospheric jet–front systems. The spontaneous grav-

ity wave emission was examined theoretically by Ford et al. (2000) for the unbounded f-plane shallow-water flow system and by Vanneste and Yavneh (2004) for a three-dimensional Boussinesq equation system.

To explore the possibility of spontaneous generation of gravity waves around the PNJ, we examined distribution of two parameters describing the degree of imbalance of the large-scale flow over the Antarctic using NCEP–NCAR reanalysis data. One is the local Rossby number Ro, which is a nondimensional number describing departure from the geostrophic balance. We used Ro defined as the absolute value of the relative vorticity ζ to planetary vorticity f (Pedlosky 1987). We also calculated the residual of the nonlinear balance equation (ΔNBE; e.g., Zhang et al. 2001), which is defined as

$$\Delta\text{NBE} = 2J(u, v) + f\zeta - \nabla^2\Phi - \beta u, \qquad (9)$$

where $\beta = \partial f/\partial y$ and Φ is the geopotential.

Figure 10 shows the results for the 30-hPa level at 1500 LST 22 June 2002 and at 2100 LST 25 June 2002, when and where gravity wave packets are observed (see the rectangles in Fig. 8). The contours show the geopotential height field. It is clear that large Ro and $|\Delta$NBE$|$ values are observed around the PNJ, which is situated at slightly lower latitudes than Syowa Station (noted with an X). This feature shows that the PNJ is unbal-
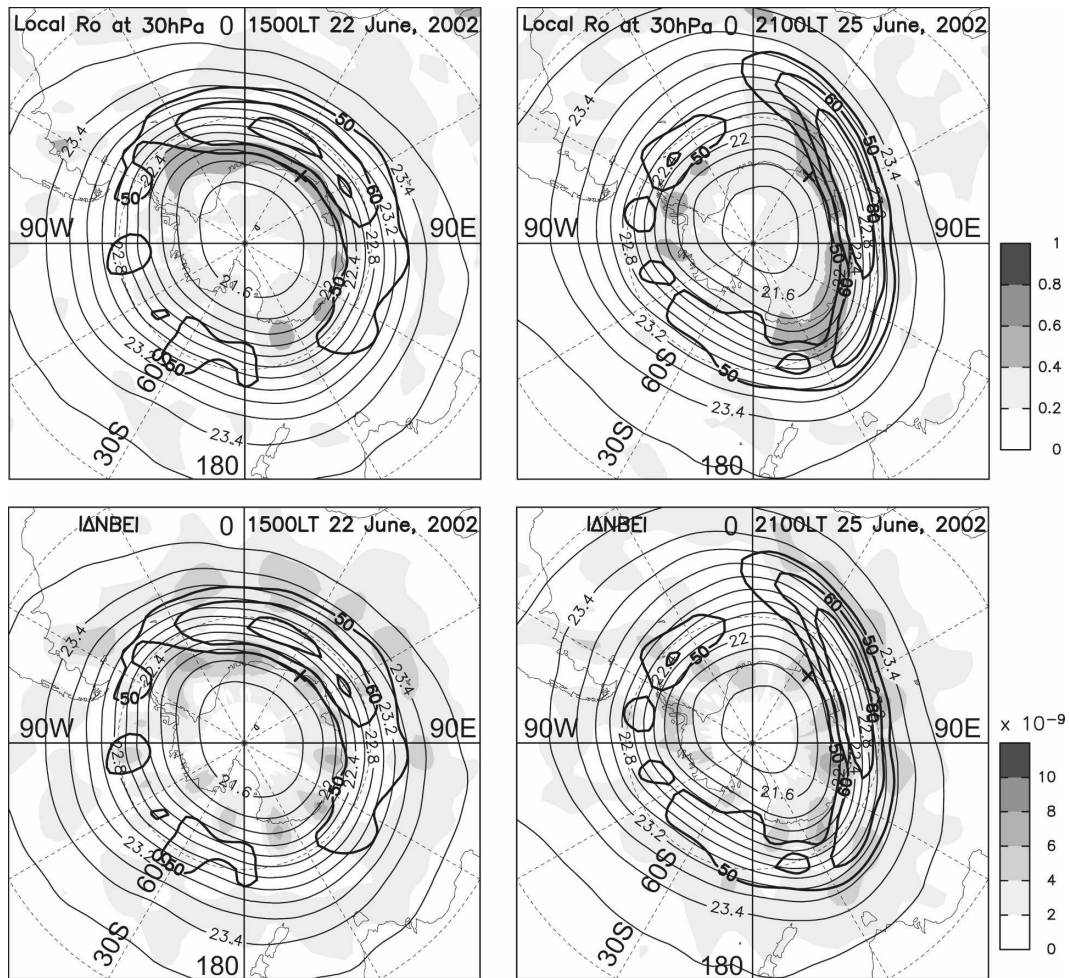
FIG. 10. (top) A polar stereo projection map of the local Rossby number and (bottom) the absolute value of the nonlinear balance equation residual at 30 hPa at (left) 1500 LST 22 Jun and (right) 2100 LST 25 Jun 2002, calculated from NCEP–NCAR reanalysis data. Thin contours indicate geopotential heights (in km) with an interval of 300 m; thick contours indicate the magnitude of horizontal winds (50, 60, and 70 m s^{-1}). Cross marks indicate location of Syowa Station.

anced and is consistent with the possibility that the gravity waves observed at Syowa Station were spontaneously generated around the unbalanced region of the PNJ. The rightward (poleward) propagation relative to the background (westerly) wind estimated by the hodograph analysis (Fig. 9) also supports this inference. The location of Syowa Station was in the exit region of the westerly jet on 22 June, but not on 25 June.

Another possible mechanism of gravity wave generation inside the fluid is the shearing instability (Fritts 1984b; Scinocca and Ford 2000). The Richardson number $[N^2/(u_z^2 + v_z^2)]$ estimated using radiosonde data was about 6 near the wave packet, which is much larger than the threshold value of 0.25 for the shearing instability. Thus, gravity wave generation due to the shearing instability is unlikely.

c. Comparison with gravity waves resolved by an aqua-planet model

Only a few simulations of gravity wave generation in the stratosphere have been performed. Fairlie et al. (1990) simulated inertia–gravity waves generated in the stratosphere during major warmings using a global model with a regular 5° × 5° latitude–longitude grid and vertical resolution of about 2 km in the stratosphere. SKT99 reported gravity wave generation in the polar vortex that is not strongly disturbed, using a gravity wave–resolving T106L53 GCM as described in section 1. Note that the horizontal and vertical resolutions of the models used in these studies are not very high by present standards and are insufficient to simulate wide horizontal and vertical wavenumber ranges of the grav-
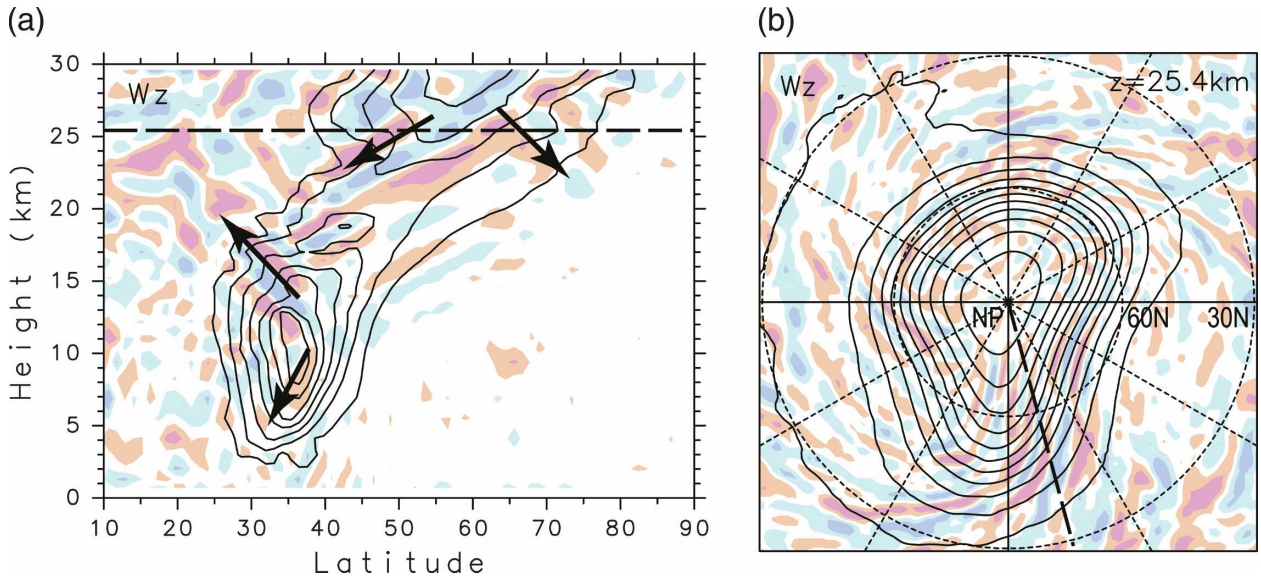
FIG. 11. Horizontal divergence components in the Northern Hemisphere simulated by a gravity wave resolving aqua-planet model with perpetual February condition. Positive and negative values are shown by warm and cold colors, respectively. (a) A latitude–height section along a longitude denoted by a thick dashed line in (b). Solid curves are contours of the horizontal wind speed. Contour intervals are 10 m s^{-1}. Arrows depict energy propagation direction. (b) A polar stereo projection map around the log-pressure height of 25.4 km denoted by a thick solid line in (a). Solid curves show geopotential heights with the same intervals of 200 m around the log-pressure height of 25.4 km.

ity wave spectrum. As reported by O'Sullivan and Dunkerton (1995) and Plougonven and Snyder (2005), the wavelengths of simulated gravity waves are largely affected by the model resolution. However, they also showed that the location of gravity wave generation is robust even in low-resolution models. Thus, we compare gravity waves observed in June with the simulation by SKT99.

Using the data from model simulation by SKT99, we examined the phase structures of the horizontal divergence components, which are mostly caused by gravity waves in the stratosphere, and the distribution of the local Rossby number and |ΔNBE| around the PNJ.

Figure 11a shows a snapshot of the latitude–height section of unfiltered horizontal divergence components along a longitude. The vertical axis shows the height in the log-pressure coordinate. The positive and negative signs of the divergence are shown by warm and cold colors, respectively. The contours show horizontal wind speeds greater than or equal to 30 m s^{-1} with an interval of 10 m s^{-1}. The middle-latitude jet stream around the tropopause is located around a height of 10 km and a latitude of 35°, and the stratospheric polar night jet is situated around a latitude of 60°.

A clear wave structure is observed for the horizontal divergence around the PNJ. Because the phase lines are parallel to the wavenumber vector of the gravity wave in this cross section, observed phase alignments indi-

cate that the gravity waves propagate downward in the vertical and poleward and equatorward in the horizontal from the PNJ. The downward energy propagation was confirmed by the sign of the vertical energy flux (not shown). The gravity wave structure is also clear around the middle-latitude jet. The gravity waves propagate equatorward in the horizontal and upward and downward in the vertical from the higher-latitude side of the middle-latitude jet. This feature is consistent with a case study by Hirota and Niki (1986) and a statistical study by Sato (1994) based on MU radar observations.

Figure 11b shows a polar stereo projection map of the horizontal wind divergence around a height of 25.4 km at the same time as shown in Fig. 11a. Contours show the geopotential height with the same intervals as in Fig. 10 (200 m). It is seen that the PNJ is distorted mostly by planetary waves. An interesting feature is that strong fluctuations of the horizontal divergence are observed in the largely distorted PNJ region. The local Rossby number and |ΔNBE| at the same time and level is shown in Fig. 12. The largely distorted region corresponds to the region with large Rossby number and |ΔNBE|. These features suggest that gravity wave generation occurs around the PNJ through spontaneous adjustment.

It is important that the distribution of large local Rossby number and |ΔNBE| associated with the PNJ in
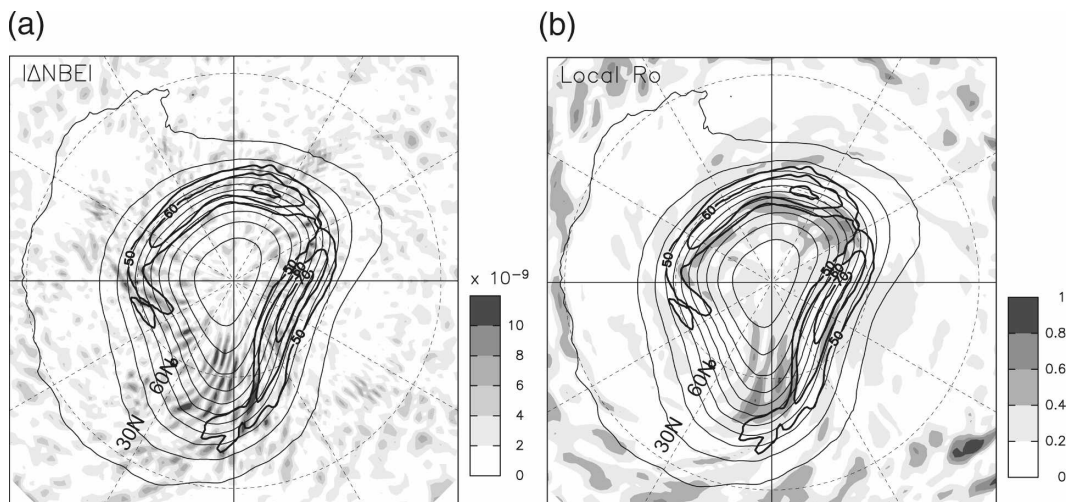
(a)

(b)

FIG. 12. As in Fig. 11b, but for (a) the absolute value of the nonlinear balance equation residual and (b) the local Rossby number. The shadings are as in Fig. 10. Thick contours show the magnitude of horizontal winds (50, 60, and 70 m s⁻¹).

the model is quite similar to the observation shown in Fig. 10. Some of the phase alignments of simulated gravity waves are consistent with observations. Therefore, it is most likely that gravity waves observed at Syowa Station in June in 2002 are generated spontaneously around the unbalanced polar night jet stream in the stratosphere.

7. Summary

Intensive radiosonde observations were performed at Syowa Station (69.0°S, 39.6°E) over about 10 days every 3 h for each of March, June, October, and December in 2002 to examine gravity wave characteristics in the Antarctic lower stratosphere. Two-dimensional (vertical wavenumber versus frequency) spectra of wind fluctuations were examined. Downward phase propagation components were dominant in all months, suggesting upward energy propagation of gravity waves. An interesting feature was the existence of clear signals of upward phase propagation in June and October, indicating that gravity waves propagated energy downward when the polar night jet was present. There was an isolated peak around the inertial frequency in a wide range of vertical wavenumbers in December when the background wind was weak, and large spectral densities were extended to lower frequencies in June and October. These features were consistent with the results by SKT99 obtained using a gravity wave–resolving global circulation model.

Detailed examinations were made of gravity waves observed in June. Dynamical characteristics were ex-

amined separately for upward- and downward-propagating gravity waves, using a hodograph analysis method. It was seen that upward- and downward-propagating wave packets occurred simultaneously in the same height regions and that they had similar horizontal wavelengths and horizontal phase velocities. This fact suggests that the sources of the upward- and downward-propagating gravity waves were the same. When the wave packets were observed, the local Rossby numbers and the residual in the nonlinear balance equation, which are measures of departure of the geostrophic balance, estimated using NCEP–NCAR reanalysis data, were large around the PNJ situated slightly to the lower latitudes of Syowa Station. Judged from these observational facts, it was concluded that the gravity waves observed at Syowa Station were generated spontaneously around the geostrophically unbalanced PNJ and propagated toward Syowa Station. The possibility of gravity wave generation around the PNJ was confirmed also by comparison with the gravity wave simulation by SKT99.

It is expected that, in the real atmosphere, significant numbers of gravity waves are generated spontaneously in strong flows, such as the westerly jet near the middle latitude tropopause and the polar night jet, and propagate both vertically and horizontally. These gravity waves may contribute to the momentum balance at higher altitudes than the source level; hence, their effects need to be parameterized in climate models. Because these waves have large horizontal wind fluctuations, their contribution to the mixing of minor constituents may be also important. However, our knowl-

edge of the dynamics of such gravity waves generated spontaneously in flows is not sufficient. In the future, detailed examinations using gravity wave–resolving high-resolution models with idealized and realistic conditions will be necessary. The reality of simulated gravity waves needs to be confirmed by observations with similar high resolutions, such as MST radar observations for the stratosphere in the middle- and high-latitude regions.

REFERENCES

Baldwin, M. P., and Coauthors, 2001: The Quasi-Biennial Oscillation. *Rev. Geophys.,* **39,** 179–229.

Carslaw, K. S., T. Peter, J. T. Bacmeister, and S. D. Eckermann, 1999: Widespread solid particle formation by mountain waves in the Arctic stratosphere. *J. Geophys. Res.,* **104,** 1827–1836.

Dunkerton, T. J., 1997: The role of gravity waves in the quasi-biennial oscillation. *J. Geophys. Res.,* **102,** 26 053–26 076.

Fairlie, T. D. A., M. Fisher, and A. O'Neill, 1990: The development of narrow baroclinic zones and other small-scale structures in the stratosphere during simulated major warmings. *Quart. J. Roy. Meteor. Soc.,* **116,** 287–315.

Ford, R., M. E. McIntyre, and W. A. Norton, 2000: Balance and the slow quasimanifold: Some explicit results. *J. Atmos. Sci.,* **57,** 1236–1254.

Fritts, D. C., 1984a: Gravity wave saturation in the middle atmosphere: A review of theory and observations. *Rev. Geophys.,* **22,** 275–308.

——, 1984b: Shear excitation of atmospheric gravity waves. Part II: Nonlinear radiation from a free shear layer. *J. Atmos. Sci.,* **41,** 524–537.

——, and M. J. Alexander, 2003: Gravity wave dynamics and effects in the middle atmosphere. *Rev. Geophys.,* **41,** 1003, doi:10.1029/2001RG000106.

Fukao, S., T. Sato, T. Tsuda, S. Kato, K. Wakasugi, and T. Makihira, 1985: The MU radar with an active phased array system. 1. Antenna and power amplifiers. *Radio Sci.,* **20,** 1155–1168.

Gardner, C. S., and N. F. Gardner, 1993: Measurement distortion in aircraft, space shuttle, and balloon observations of atmospheric density and temperature perturbation spectra. *J. Geophys. Res.,* **98,** 1023–1033.

Haynes, P. H., 1998: The latitudinal structure of the quasi-biennial oscillation. *Quart. J. Roy. Meteor. Soc.,* **124,** 2645–2670.

——, C. J. Marks, M. E. McIntyre, T. G. Shepherd, and K. P. Shine, 1991: On the "downward control" of extratropical diabatic circulations by eddy-induced mean zonal forces. *J. Atmos. Sci.,* **48,** 651–678.

Hines, C. O., 1989: Tropopausal mountain waves over Arecibo: A case study. *J. Atmos. Sci.,* **46,** 476–488.

Hio, Y., and S. Yoden, 2005: Interannual variations of the seasonal march in the Southern Hemisphere stratosphere for 1979–2002 and characterization of the unprecedented year 2002. *J. Atmos. Sci.,* **62,** 567–580.

Hirota, I., and T. Niki, 1986: Inertia–gravity waves in the troposphere and stratosphere observed by the MU radar. *J. Meteor. Soc. Japan,* **64,** 995–999.

Höpfner, M., and Coauthors, 2006: MIPAS detects Antarctic stratospheric belt of NAT PSCs caused by mountain waves. *Atmos. Chem. Phys.,* **6,** 1221–1230.

Lane, T. P., M. J. Reeder, B. R. Morton, and T. L. Clark, 2000: Observations and numerical modelling of mountain waves over the Southern Alps of New Zealand. *Quart. J. Roy. Meteor. Soc.,* **126,** 2765–2788.

Lilly, D., and P. Kennedy, 1973: Observations of a stationary mountain wave and its associated momentum flux and energy dissipation. *J. Atmos. Sci.,* **30,** 1135–1152.

Lindzen, R. S., 1981: Turbulence and stress owing to gravity wave and tidal breakdown. *J. Geophys. Res.,* **86,** 9707–9714.

Lintelman, S. A., and C. S. Gardner, 1994: Observation and interpretation of spectra of atmospheric gravity wave perturbations with upward and downward phase progression. *J. Geophys. Res.,* **99,** 16 959–16 972.

Mann, G. W., K. S. Carslaw, M. P. Chipperfield, S. Davies, and S. D. Eckermann, 2005: Large nitric acid trihydrate particles and denitrification caused by mountain waves in the Arctic stratosphere. *J. Geophys. Res.,* **110,** D08202, doi:10.1029/2004JD005271.

Matsuno, T., 1982: A quasi-one-dimensional model of the middle atmosphere circulation interacting with internal gravity waves. *J. Meteor. Soc. Japan,* **60,** 215–226.

McFarlane, N. A., 1987: The effect of orographically excited gravity wave drag on the general circulation of the lower stratosphere and troposphere. *J. Atmos. Sci.,* **44,** 1775–1800.

Nash, E. R., P. A. Newman, J. E. Rosenfield, and M. R. Schoeberl, 1996: An objective determination of the polar vortex using Ertel's potential vorticity. *J. Geophys. Res.,* **101,** 9471–9478.

Nastrom, G. D., and F. D. Eaton, 2006: Quasi-monochromatic inertia–gravity waves in the lower stratosphere from MST radar observations. *J. Geophys. Res.,* **111,** D19103, doi:10.1029/2006JD007335.

O'Sullivan, D., and T. J. Dunkerton, 1995: Generation of inertia–gravity waves in a simulated life cycle of baroclinic instability. *J. Atmos. Sci.,* **52,** 3695–3716.

Palmer, T. N., G. J. Shutts, and R. Swinbank, 1986: Alleviation of a systematic westerly bias in general circulation and numerical weather prediction models through an orographic gravity wave drag. *Quart. J. Roy. Meteor. Soc.,* **112,** 1001–1039.

Pedlosky, J., 1987: *Geophysical Fluid Dynamics.* 2nd ed. Springer, 128 pp.

Pfenninger, M., A. Z. Liu, G. C. Papen, and C. S. Gardner, 1999: Gravity wave characteristics in the lower atmosphere at the South Pole. *J. Geophys. Res.,* **104,** 5963–5984.

Plougonven, R., and C. Snyder, 2005: Gravity waves excited by jets: Propagation versus generation. *Geophys. Res. Lett.,* **32,** L18802, doi:10.1029/2005GL023730.

——, and ——, 2007: Inertia–gravity waves spontaneously generated by jets and fronts. Part I: Different baroclinic life cycles. *J. Atmos. Sci.,* **64,** 2502–2520.

Plumb, R. A., 2002: Stratospheric transport. *J. Meteor. Soc. Japan,* **80,** 793–809.

Sato, K., 1989: An inertial gravity wave associated with a synoptic-scale pressure trough observed by the MU radar. *J. Meteor. Soc. Japan,* **67,** 325–334.

——, 1994: A statistical study of the structure, saturation and sources of inertio-gravity waves in the lower stratosphere observed with the MU radar. *J. Atmos. Terr. Phys.,* **56,** 755–774.

——, 2000: Sources of gravity waves in the polar middle atmosphere. *Adv. Polar Upper Atmos. Res.,* **14,** 233–240.

——, and T. J. Dunkerton, 1997: Estimates of momentum flux associated with equatorial Kelvin and gravity waves. *J. Geophys. Res.,* **102,** 26 247–26 261.

——, D. J. O'Sullivan, and T. J. Dunkerton, 1997: Low-frequency inertia–gravity waves in the stratosphere revealed by three-week continuous observation with the MU radar. *Geophys. Res. Lett.,* **24,** 1739–1742.

——, T. Kumakura, and M. Takahashi, 1999: Gravity waves appearing in a high-resolution GCM simulation. *J. Atmos. Sci.,* **56,** 1005–1018.

Scinocca, J. F., and R. Ford, 2000: The nonlinear forcing of large-scale internal gravity waves by stratified shear instability. *J. Atmos. Sci.,* **57,** 653–672.

Shibata, T., K. Sato, H. Kobayashi, M. Yabuki, and M. Shiobara, 2003: The Antarctic polar stratospheric clouds under the temperature perturbation by nonorographic inertia–gravity waves observed by micropulse lidar. *J. Geophys. Res.,* **108,** 4105, doi:10.1029/2002JD002713.

Tanaka, H., and M. D. Yamanaka, 1985: Atmospheric circulation in the lower stratosphere induced by the mesoscale mountain wave breakdown. *J. Meteor. Soc. Japan,* **63,** 1047–1054.

Vanneste, J., and I. Yavneh, 2004: Exponentially small inertia–gravity waves and the breakdown of quasigeostrophic balance. *J. Atmos. Sci.,* **61,** 211–223.

Venkat Ratnam, M., T. Tsuda, C. Jacobi, and Y. Aoyama, 2004: Enhancement of gravity wave activity observed during a major Southern Hemisphere stratospheric warming by CHAMP/GPS measurements. *Geophys. Res. Lett.,* **31,** L16101, doi:10.1029/2004GL019789.

Wang, S., and F. Zhang, 2007: Sensitivity of mesoscale gravity waves to the baroclinicity of jet-front systems. *Mon. Wea. Rev.,* **135,** 670–688.

Watanabe, S., K. Sato, and M. Takahashi, 2006: A general circulation model study of the orographic gravity waves over Antarctica excited by katabatic winds. *J. Geophys. Res.,* **111,** D18104, doi:10.1029/2005JD006851.

Yoshiki, M., and K. Sato, 2000: A statistical study of gravity waves in the polar regions based on operational radiosonde data. *J. Geophys. Res.,* **105,** 17 995–18 011.

——, N. Kizu, and K. Sato, 2004: Energy enhancements of gravity waves in the Antarctic lower stratosphere associated with variations in the polar vortex and tropospheric disturbances. *J. Geophys. Res.,* **109,** D23104, doi:10.1029/2004JD004870.

Zhang, F., 2004: Generation of mesoscale gravity waves in the upper-tropospheric jet–front systems. *J. Atmos. Sci.,* **61,** 440–457.

——, S. E. Koch, C. A. Davis, and M. L. Kaplan, 2001: Wavelet analysis and the governing dynamics of a large-amplitude mesoscale gravity-wave event along the East Coast of the United States. *Quart. J. Roy. Meteor. Soc.,* **127,** 2209–2245.